A&A 544, A153 (2012)
DOI: 10.1051/0004-6361/201219309

Astronomy
&
Astrophysics

Using electromagnetic observations to aid gravitational-wave parameter estimation of compact binaries observed with LISA

S. Shah[1,2], M. van der Sluys[1,2], and G. Nelemans[1,2,3]

[1] Department of Astrophysics/ IMAPP, Radboud University Nijmegen, PO Box 9010, 6500 GL Nijmegen, The Netherlands
e-mail: `s.shah@astro.ru.nl`
[2] Nikhef National Institute for Subatomic Physics, Science Park 105, 1098 XG Amsterdam, The Netherlands
[3] Institute for Astronomy, KU Leuven, Celestijnenlaan 200D, 3001 Leuven, Belgium

Received 29 March 2012 / Accepted 17 June 2012

ABSTRACT

We present a first-stage study of the effect of using knowledge from electromagnetic (EM) observations in the gravitational wave (GW) data analysis of Galactic binaries that are predicted to be observed by the new Laser Interferometer Space Antenna (LISA) in the low-frequency range, 10^{-4} Hz $< f <$ 1 Hz. In particular, we examine the extent to which the accuracy of GW parameter estimation improves if we use available information from EM data. We do this by investigating whether correlations exist between the GW parameters that describe these binaries and whether some of these parameters are also available from EM observations. We used verification binaries, which are known as the guaranteed sources for eLISA and will test the functioning of the instrument. We find that of the seven parameters that characterise such a binary, only a few are correlated. The most useful result is the strong correlation between amplitude and inclination, which can be used to constrain the parameter uncertainty in amplitude by making use of the constraint of inclination from EM measurements. The improvement can be up to a factor of ~6.5, but depends on the signal-to-noise ratio of the source data. Moreover, we find that this strong correlation depends on the inclination. For mildly face-on binaries ($\iota \lesssim 45°$), EM data on inclination can improve the estimate of the GW amplitude by a significant factor. However, for edge-on binaries ($\iota \sim 90°$), the inclination can be determined accurately from GW data alone, thus GW data can be used to select systems that will likely be eclipsing binaries for EM follow-up.

Key words. binaries: general – gravitational waves

1. Introduction

The space-based gravitational wave (GW) detector in consideration by ESA, eLISA, is expected to observe millions of compact Galactic binaries (Nelemans 2009; Amaro-Seoane et al. 2012) with periods shorter than about a few hours, amongst other astrophysical sources, and resolve several thousand of these binaries (Nissanke et al. 2012). About 50 compact binary sources have been observed at optical, UV, and X-ray wavelengths (e.g. Roelofs et al. 2010). The types of binaries known to us are interacting systems (AM CVn stars, ultra-compact X-ray binaries, and cataclysmic variables) and detached systems (double white dwarfs (WDs) and double neutron stars, Nelemans 2009, 2011). The AM CVn stars are binary systems where a WD accretes matter from a low-mass, helium-rich (hydrogen-deficient) object (Solheim 2010). Their mass transfer is driven by GW radiation loss. The known ultra-compact X-ray binaries consist of neutron stars that are accretors whose donors are inferred to be either helium rich or carbon/oxygen rich (in't Zand 2005). Double WDs are predicted to be the most common systems, which sometimes tend to be the outcome of many binary evolutionary paths (Webbink 1984). Of all these known systems, a handful lie in the eLISA band and will be individually detected. These are known as *verification binaries* since they are guaranteed sources for the detector. Parameter uncertainties in the verification binaries and Galactic binaries in general have been studied in the literature by extensively using Fisher information matrix (FIM) analyses (e.g. Cutler 1998; Takahashi & Seto 2002; Stroeer & Vecchio 2006). These studies have been done for various configurations of classic LISA (LISA Study Team 1998), which was designed to have a larger baseline of five million km with six laser links interchanging between three stations located at the vertices of a triangle that was to house two proof masses each (Vallisneri et al. 2008). Instead eLISA will have a baseline of one million km with four laser links interchanging between the proof masses. The parameter uncertainties depend intricately on the observation conditions and the geometry of the detector (Takahashi & Seto 2002) and the same is true for the (possible) correlations between the parameters of a Galactic binary. In this study, we wish to quantify whether any such correlations exist that could be useful in constraining the GW parameter estimates. Some of the GW parameters are the same as or related to electromagnetic (EM) parameters (e.g. $\text{inclination}_{\text{GW}} = \text{inclination}_{\text{EM}}$, $f_{\text{GW}} = 2/P_{\text{orb}}$, etc.). Thus, we can use an independent (EM) constraint of a (EM/GW) parameter that correlates strongly with another (GW) parameter to improve the accuracy of the latter. This work provides a first step towards developing strategic plans in observing those potentially useful EM parameters that can improve the GW parameter accuracy. In this paper, we present a FIM analysis to study whether correlations within GW parameters exist. For the useful correlations that we find, we predict quantitatively the improvement in the GW parameter when there is *prior* EM data in the correlated parameter. The paper is structured in the following way. In Sect. 2, we briefly summarise the signal models, both the instrumental and foreground noises, and our data analysis. We present our results and interpretations in Sect. 3. Finally, we discuss how the results differ from the old LISA detector in Sect. 4 and present our conclusions in Sect. 5.

Table 1. Physical properties of verification binaries based on observations summarised in Nelemans (2011).

	S/N	$m_1[M_\odot]$	$m_2[M_\odot]$	d[kpc]	$\mathcal{A}^*[\times 10^{-22}]$	$P_{\rm orb}$[s]	$\iota[°]$	$\dot{P}_{\rm orb}$[s/s]	β[rad]	λ[rad]
J0651	10.7	0.55^a	0.25^a	$\sim 1^a$	1.67	765.4 ± 7.9^a	$86.9^{+1.6a}_{-1}$	–	0.101	1.769
AM CVn	11.5	0.71^b	0.13^b	$0.606^{+0.135c}_{-0.93}$	1.49	1028.73^d	43 ± 2^c	–	0.653	2.974
HM Cnc	39.7	0.55^e	0.27^e	5^e	6.38	321.529^f	$\approx 38^e$	3.75×10^{-11f}	−0.082	2.102

Notes. The signal-to-noise ratio (S/N) listed in the second column is from GW data analysis, as explained in Sect. 3. (a) Brown et al. (2011); (b) Roelofs et al. (2006); (c) Roelofs et al. (2007); (d) Skillman et al. (1999); (e) Roelofs et al. (2010); (f) Strohmayer (2005); (*) Eq. (3).

2. Signal modelling and data analysis

2.1. Gravitational wave signals from a Galactic binary

We consider three verification sources, AM CVn, SDSS J0651+2844 (hereafter J0651), and RX J0806.3+1527 (HM Cnc), whose physical parameters are summarised in Table 1.

AM CVn and HM Cnc are mass-transferring systems known to astronomers as AM CVn binary systems, which were described in the introduction. J0651 (Brown et al. 2011) is an eclipsing detached WD binary system that was spectroscopically identified in the Sloan Digital Sky Survey (SDSS) catalogue. AM CVn and J0651 can be modelled as monochromatic GW sources, which means that they are described by seven parameters: dimensionless amplitude ($\mathcal{A}$), frequency (f), polarisation angle (ψ), initial GW phase (ϕ_0), inclination ($\cos\iota$), ecliptic latitude ($\sin\beta$), and ecliptic longitude (λ). HM Cnc can be modelled as a mild chirper with an additional eighth parameter, the chirping frequency ($\dot{f}$). The two polarised gravitational waveforms used in the strain for slowly evolving binaries are given by (e.g. Królak et al. 2004)

$$h_+(t) = \mathcal{A}\,\frac{1+\cos^2\iota}{2}\,\cos\left(2\pi f t + \pi \dot{f} t^2 + \phi_0\right); \tag{1}$$

$$h_\times(t) = \mathcal{A}\,\cos\,\iota\,\,\sin\left(2\pi f t + \pi \dot{f} t^2 + \phi_0\right), \tag{2}$$

where

$$\mathcal{A} = \frac{4(G\,\mathcal{M})^{5/3}}{c^4\,d}(\pi f)^{2/3} \tag{3}$$

and

$$\dot{f} = \frac{96}{5}\frac{f}{\mathcal{M}}(\pi f \mathcal{M})^{8/3}. \tag{4}$$

In these expressions, $\mathcal{M} \equiv (m_1 m_2)^{3/5}/(m_1+m_2)^{1/5}$ is the chirp mass and d is the distance to the source. The monochromatic waveforms are given by setting $\dot{f} = 0$ in the expressions above.

2.2. Detector response to the GW signals

If a GW signal is present, then the output of a detector will contain the strain, $h(t)$, and noise, $n(t)$. Thus, the detector registers

$$s(t) = h(t;\boldsymbol{\theta}) + n(t), \tag{5}$$

where $\boldsymbol{\theta}$ is a vector characterising the seven (or eight) parameters of the binary. Since eLISA will have a motion around the Sun and a cartwheeling motion around its centre of mass, a monochromatic signal from a WD binary will be modulated in its amplitude, frequency, and phase in complicated ways. The resulting signal will be spread over a range of frequency bins of the detector (Cornish & Larson 2003). Galactic binaries typically radiate monochromatic signals at low frequencies[1] and thus the response at the detector can be written as (Cornish & Larson 2003)

$$h(t) = A(t)\,\cos\Psi(t), \tag{6}$$

where

$$A(t) = \left[(F^+(t)h_+(t))^2 + (F^\times(t)h_\times(t))^2\right]^{1/2}. \tag{7}$$

The functions $F^{+,\times}(t)$ are the antenna beam patterns of the detector, and they depend on the source's sky position (λ, β), its orientation (ψ), and the detector configuration. The phase of the signal is given by

$$\Psi(t) = 2\pi f t + \phi_0 + \Phi_{\rm D}(t) + \Phi_{\rm P}(t), \tag{8}$$

where $\Phi_{\rm D}(t), \Phi_{\rm P}(t)$ are frequency (Doppler) and phase modulations, respectively (Cornish & Larson 2003). Doppler modulation is given by

$$\Phi_{\rm D}(t) = 2\pi f L/c\quad \sin\beta\,\,\cos(2\pi f_{\rm m} t - \lambda), \tag{9}$$

where $f_{\rm m} = 1/\text{year}$ is the modulation frequency. The phase modulation is given by

$$\Phi_{\rm P}(t) = -\arctan\left(\frac{F^\times\,h_\times}{F^+\,h_+}\right). \tag{10}$$

Different architectures of the triangular space-based interferometer generate a number of independent data streams that provide different responses to the incoming GW signal (Vallisneri et al. 2008). For the most recent interferometer design in consideration, eLISA, the output is a single unequal-arm Michelson data stream, X. This is a linear combination of phase shifts measured at the different spacecraft (by comparing the incoming light with a local reference source) shifted in time in such a way as to represent interference between two light beams travelling through the arms of the detector in opposite ways, which is a particular implementation of so-called time delay interferometry (TDI, Armstrong et al. 1999). Vallisneri (2005a) provide a detailed description of how TDI works and an explanation of why it produces an interferometry signal in which the phase shift induced by a passing GW is preserved, while the much larger shifts induced by instrumental noise are strongly suppressed. We made use of the existing numerical software *Synthetic LISA* (Vallisneri 2005b) to simulate accurate time-domain series of the instrumental noise and the GW signals in the form of these TDI observables. The data stream is a discrete series for a given observational time $T_{\rm obs}$, where the samples are separated by Δt. The

---

[1] Low f is a function of the detector transfer frequency, f_*,$f \ll f_*$. The f_* is defined according to the detector armlength, L, i.e. $f_* \equiv c/(2\pi L)$. For eLISA, $L = 10^9$ m, $f_* \approx 5 \times 10^{-2}$ Hz.

detector response to GWs and instrumental noises have been discussed extensively in the literature (e.g. Cutler 1998; Cornish & Rubbo 2003; Królak et al. 2004; Vallisneri 2005b), hence we only summarise the most essential expressions relevant to our data analysis. In *Synthetic LISA*, the strain at the detector, $s(t)$, is modelled as the TDI X observable. This is the quantity we work with in our data analysis.

2.3. Noise

There are two types of noise to consider: instrumental noise and Galactic foreground noise due to unresolved compact binaries. For the particular geometry of eLISA used here, the instrumental noises (mostly from shot noise), acceleration noise, and other types of noise (e.g. optical bench noise), are characterised by their power spectral densities (PSDs[2]) of $2.31 \times 10^{-38} f^2$, $6 \times 10^{-48} f^{-2}$, and $2.76 \times 10^{-38} f^2$, respectively, in units of Hz^{-1}. The instrumental noise is modelled as a random, Gaussian process. We note that the sampling time, Δt, should be carefully chosen while simulating the instrumental noise in order to correctly interpret the TDI observables. The choice of Δt should correspond to a frequency that is several times higher than the highest frequency where the TDI responses have to be analysed (Vallisneri 2005b). This means that since AM CVn and J0651 have relatively low frequencies they can be analysed with samples of $\Delta t = 64$ s, whereas for HM Cnc, we need a lower sampling time of at least $\Delta t = 16$ s (see Fig. B.1 in Appendix B).

The foreground noise from the Galactic binaries is simulated using the *Lisasolve* (Vallisneri 2011) software where every binary (monochromatic and/or mild chirper[3]) is modelled in the frequency domain (Cornish & Littenberg 2007). This differs from simulating signals using *Synthetic LISA*, where the signal is modelled accurately in the time-domain. *Lisasolve* instead makes use of the very slowly evolving nature of the binaries to approximately model the signals both directly and speedily in the frequency domain. We only use double-detached WD binaries because they form the majority of the foreground noise (Nelemans et al. 2001; Petiteau 2012). We include more than 2.7×10^7 detached Galactic double WDs from a simulation with the same assumptions about binary evolution and Galactic distribution as those in Nelemans et al. (2004), but with (about a factor of ten) higher intrinsic resolution. These assumptions have also been used for the simulations of the Galactic binaries on which the Mock LISA Data Challenge (MLDC) rounds are based (Littenberg 2011).

The *unresolvable* Galactic foreground noise is obtained by iteratively subtracting the *resolvable* sources (i.e. binaries expected to be detected) from the simulated population as follows:

1. the S/N (see Eq. (14)) is computed for each binary against the Gaussian instrumental noise and *initial* Galactic foreground noise for $T_{\rm obs}$ of two years. The initial foreground noise is calculated using the initial catalogue of 2.7×10^7 detached Galactic double WDs;
2. all the sources with $S/N > 5$ are removed from the initial catalogue/dataset. The *reduced* dataset is used to simulate the reduced Galactic foreground;
3. using the reduced Galactic foreground and the same instrumental noise, the S/N for each of the binaries in the reduced catalogue is calculated. The process is iterated with step 2.

We applied a perfect subtraction of the bright sources where any spurious effects in the data set were not taken into account (since the sources were removed from the population before generating the signals). A Markov chain Monte Carlo (MCMC) based data analysis of the MLDC shows that all the recovered parameters of the subtracted sources have a strong peak of zero bias when compared to their injected values in the training data set (Littenberg 2011). Thus, this perfect subtraction scheme is not expected to introduce strong biases in our results. From our subtraction procedure outlined above, we estimate the number of resolved WD binaries to be ~11 000. Using the same subtraction procedure and S/N threshold, Nissanke et al. (2012) estimate the number of bright sources to be half of our estimate, although their estimate is only for a $T_{\rm obs}$ of one year. Furthermore, using a higher S/N threshold of seven, the number of resolvable sources is 3000 for an observation time of two years (Amaro-Seoane et al. 2012). If we use a threshold S/N of seven, we find 4500 resolvable sources. The PSD of the unresolvable Galactic background is consistent with findings in the literature where the foreground noise for eLISA is almost at the level of instrumental noise for this detector (Nissanke et al. 2012), unlike in the case of the classic LISA where the foreground noise was predicted to dominate at $f \lesssim 3$ mHz (Nelemans et al. 2001; Timpano et al. 2006).

2.4. Data analysis

For GW sources with known waveforms, one can use matched filtering methods (Finn 1992; Cutler & Flanagan 1994) to extract the signal parameters and estimate their uncertainties. Consequently, when the noise is Gaussian, the parameter uncertainties are given by their joint Gaussian probability distribution function (Cutler 1998)

$$p(\sigma_{\boldsymbol\theta}) = \sqrt{\det(\Gamma/2\pi)}\ \exp\left(-\frac{1}{2}\,\Gamma_{ij}\,\sigma_{\theta_i}\,\sigma_{\theta_j}\right), \tag{11}$$

where Γ is known as the Fisher information matrix (FIM) given by

$$\Gamma_{ij} \equiv \left(\frac{\partial h}{\partial \theta_i}\,\middle|\,\frac{\partial h}{\partial \theta_j}\right). \tag{12}$$

The inner product (...|...) is a generalisation of the time-domain correlation product and is conventionally defined as

$$(a|b) = 4\int_0^\infty \mathrm{d}f\,\frac{\tilde a^*(f)\,\tilde b(f)}{S_n(f)} \simeq \frac{2}{S_n(f_0)}\int_0^{T_{\rm obs}} \mathrm{d}t\ a(t)\,b(t). \tag{13}$$

Equation (13)[4] holds for quasi-monochromatic binaries that have an almost constant noise PSD, $S_n(f)$, in the frequency region where the binary radiates (Cutler 1998). The S/N of a source is defined as the inner product of a signal with itself

$$S/N^2 = (h|h). \tag{14}$$

In the limit of signals with a high signal-to-noise ratio ($S/N \gg 1$), the inverse of the FIM gives the variance-covariance matrix $C = \Gamma^{-1}$. The diagonal elements C_{ii} give variances (or mean square errors) in each parameter, $\langle(\sigma_i)^2\rangle$, and the off-diagonal elements describe the covariances (or correlations) between them. For each of our verification binaries, we calculate this matrix to investigate the correlations between the binary parameters. The

---

[2] Note there is no PSD for laser noise, since we assume that it is completely cancelled in the TDI observable X.

[3] Mild implies that $\dot f/f \ll 1/T_{\rm obs}$, where $T_{\rm obs}$ is the observational time.

[4] The latter equality follows from Parseval's theorem.

derivative in Eq. (12), $\partial h/\partial \theta_i$, is numerically calculated in the time-domain

$$h'(t;\theta_i) \equiv \frac{h(t;\theta_i + \mathrm{d}\theta_i) - h(t;\theta_i - \mathrm{d}\theta_i)}{2\mathrm{d}\theta_i}, \tag{15}$$

where $\mathrm{d}\theta_i$ should be chosen carefully. In general, the quantity $\mathrm{d}\theta_i$ should be as small as the machine accuracy allows for, but not too large to suffer from the truncation error[5]. Thus, for well-behaved functions, $\mathrm{d}\theta_i \sim \sqrt{\epsilon}\,\theta_\mathrm{c}$, where $\epsilon \sim 10^{-16}$ is the machine accuracy and θ_c is some typical value of the corresponding parameter (Press et al. 2002). To find a good choice of $\mathrm{d}\theta_i$, we compute σ_i for a range of $\mathrm{d}\theta_i$ with logarithmic intervals and select the value for each corresponding parameter around which the standard deviations become stable. By stable, we mean that increasing or decreasing $\mathrm{d}\theta_i$ by an order of magnitude should lead to values of σ_i that vary by no greater (smaller) factor than 1.1 (0.9). An example of the stabilisation of the variance-covariance matrix is provided in Table A.1 of Appendix A for the case of AM CVn. We perform this stability check for all our verification binaries. For instance, in the case of AM CVn, $\mathrm{d}\theta_\mathcal{A} \sim 10^{-30}$, $\mathrm{d}\theta_\mathrm{f} \sim 10^{-11}$, $\mathrm{d}\theta_{\iota,\psi} \sim 10^{-8}$ etc. All our analysis is done for $T_\mathrm{obs} = 2$ years.

3. Results

Here we list the variance-covariance matrix C for AM CVn, HM Cnc, and J0651 and discuss the strongest correlations that we found. The off-diagonal elements are specified by the normalised correlations, c_{ij}, and the diagonal elements are quoted as the square root of the variances (or standard deviations), c_{ii}, i.e.

$$c_{ij} = \frac{C_{ij}}{\sqrt{C_{ii}C_{jj}}}, \quad c_{ii} = \sqrt{C_{ii}} \equiv \sigma_i. \tag{16}$$

Thus, c_{ij} can have values in the range $[-1, +1]$ where, $c_{ij} = +1$ means maximally correlated and $c_{ij} = -1$ means maximally anti-correlated. We consider highly correlated parameters θ_i, θ_j to be those for which $|c_{ij}| > 0.8$. In the later subsections, we show that these correlations are affected when the inclination is varied.

The correlation matrices for the three verification binaries with observed parameters as shown in Table 1 are listed below. The measured GW parameter values are shown above each matrix. Since there are no EM measurements for ϕ_0 and ψ, we set them to π and $\pi/2$, respectively, for all three binaries. The choice of the ϕ_0 value does not influence the results shown below, whereas the choice for the ψ has an effect that will be addressed later. In the matrices, we take the medians of values obtained using 50 different instrumental-noise realisations and the standard deviations about these medians (σ(S/N) and $\sigma(\sigma_i)$). They are listed above and below each of the corresponding matrices, respectively. The values of S/N we find here are comparable to the ones found by other groups (Petiteau 2012). The normalised correlations are accurate within the quoted precision and hence their standard deviations from the instrumental noise are not listed.

J0651, $S/N = 10.72 \pm 0.23$.

Strong correlations (as defined above) are printed in bold face.

	$\mathcal{A}$	ϕ_0	$\cos\iota$	f	ψ	$\sin\beta$	λ
θ_i	1.670×10^{-22}	π	0.01	2.614×10^{-3}	$\pi/2$	0.10	1.77
$\mathcal{A}$	1.564×10^{-23}	0.01	−0.05	−0.02	0.02	0.03	−0.08
ϕ_0		0.208	−0.01	**−0.89**	−0.02	0.13	−0.13
$\cos\iota$			0.043	0.01	0.02	−0.06	0.34
f				8.375×10^{-10}	0.01	−0.17	0.16
ψ					0.040	−0.03	0.09
$\sin\beta$						0.069	0.09
λ							0.020
$\sigma(\sigma_i)3.31 \times 10^{-25}$	0.004	0.001	1.771×10^{-11}	0.001	0.001	0.000	

AM CVn, $S/N = 11.54 \pm 0.19$.

	$\mathcal{A}$	ϕ_0	$\cos\iota$	f	ψ	$\sin\beta$	λ
θ_i	1.494×10^{-22}	π	0.73	1.944×10^{-3}	$\pi/2$	0.61	2.97
$\mathcal{A}$	1.084×10^{-22}	0.29	**−0.99**	−0.06	−0.30	−0.03	−0.60
ϕ_0		2.333	−0.27	−0.03	**−0.99**	0.26	−0.44
$\cos\iota$			0.580	0.06	0.28	0.04	0.60
f				6.807×10^{-10}	−0.03	−0.11	−0.19
ψ					1.170	−0.27	0.03
$\sin\beta$						0.029	0.03
λ							0.040
$\sigma(\sigma_i)$	1.821×10^{-24}	0.039	0.010	1.145×10^{-11}	0.020	0.000	0.001

HM Cnc, $S/N = 39.75 \pm 0.82$.

	$\mathcal{A}$	ϕ_0	$\cos\iota$	f	ψ	$\sin\beta$	λ
θ_i	6.378×10^{-23}	π	0.79	6.22×10^{-3}	$\pi/2$	−0.08	2.10
$\mathcal{A}$	1.236×10^{-23}	0.01	**−0.99**	0.00	−0.01	−0.12	0.07
ϕ_0		0.916	−0.01	−0.14	**−0.998**	−0.16	−0.08
$\cos\iota$			0.169	0.00	0.01	−0.12	−0.07
f				2.257×10^{-10}	0.09	0.29	−0.06
ψ					0.455	0.14	−0.06
$\sin\beta$						0.018	−0.06
λ							0.002
$\sigma(\sigma_i)$	2.5×10^{-25}	0.019	0.003	4.6×10^{-12}	0.009	0.000	0.000

HM Cnc, with $\dot{f}$, $S/N = 39.89 \pm 0.85$.

	$\mathcal{A}$	ϕ_0	$\cos\iota$	f	$\dot{f}$	ψ	$\sin\beta$	λ
θ_i	6.378×10^{-23}	π	0.79	6.22×10^{-3}	-7.25×10^{-16}	$\pi/2$	−0.08	2.10
$\mathcal{A}$	1.240×10^{-23}	0.0	**−0.99**	0.02	−0.02	0.00	0.15	−0.08
ϕ_0		0.907	0.00	−0.14	0.11	**0.995**	−0.02	−0.04
$\cos\iota$			0.172	−0.02	0.02	−0.01	−0.15	0.08
f				9.58×10^{-10}	**−0.97**	−0.05	−0.05	−0.28
$\dot{f}$					2.971×10^{-17}	0.04	0.14	0.28
ψ						0.448	−0.01	−0.07
$\sin\beta$							0.018	0.09
λ								0.002
$\sigma(\sigma_i)$	2.6×10^{-25}	0.019	0.004	2.1×10^{-11}	5.96×10^{-19}	0.009	0.000	0.000

3.1. *The correlation between $\mathcal{A}$ and $\cos\iota$*

The amplitude and inclination of AM CVn and HM Cnc (when modelled without the chirp, $\dot{f}$) are highly anti-correlated, with a value of $c_{\mathcal{A}\cos\iota} \approx -0.99$. The reason for this is that binaries with inclinations in the range from 0° to ~45° (face-on or close to face-on) have signals with the same structure (see Fig. 1), so the signals in this range can be transformed into each other by simply changing either the amplitude or the inclination. Thus, if we change the amplitude of one of these signals within its GW uncertainty, we can obtain a very similar signal by changing its inclination within its GW uncertainty as well. However, for inclinations in the range ~45°–90° (either close to edge-on or edge-on), this scaling does not apply. This is because the signals in this range not only vary in terms of the overall scale but also in their structure, when their inclination is changed. This is especially evident for a binary with $\iota \sim 90°$ (lines of $\iota = 60°, 90°$ in Fig. 1). Since the inclinations of both AM CVn and HM Cnc are within the range where similar signals can be obtained by varying either the inclination or the strain amplitude, the parameters $\cos\iota$ and $\mathcal{A}$ are highly correlated. Furthermore since J0561 is an edge-on system with $\iota \sim 90°$, both $\cos\iota$ and $\mathcal{A}$ are distinguishable, as can be seen in Fig. 1. This is potentially the most useful correlation from the GW analysis where an EM measurement of the inclination of a binary can constrain the error in the

---

[5] This error comes from higher-order terms in the Taylor-series expansion, $h(x + \mathrm{d}x) = h(x) + \mathrm{d}x\, h'(x) + \frac{1}{2}\,\mathrm{d}x^2\, h''(x) + \ldots$

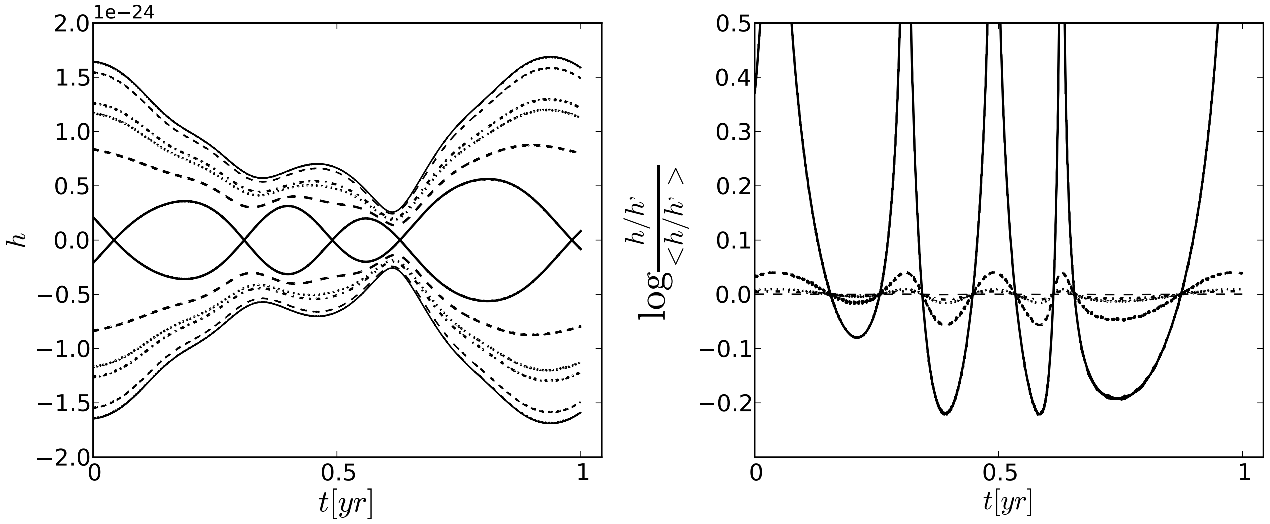

Fig. 1. *Left*: envelopes of the GW signal (TDI X observable) for binaries with parameters of AM CVn, but for various inclinations as a function of time (innermost to outermost envelopes correspond to $\iota = 90°, 60°, 45°, 40°, 20°, 0°$ respectively). The modulation of the signal is due to the complicated annual motion of eLISA around the Sun. For low inclinations ($\iota = 0°–45°$), the signals only differ in amplitude, while the higher inclinations also differ in structure. To highlight this, we plot in the right panel the normalised ratio of the upper envelopes compared to the $\iota = 0°$ envelope using the same line styles (but now the $\iota = 90°$ is the outermost line). High inclination systems clearly have a unique structure, while low inclination envelopes only differ in amplitude, illustrating the degeneracy between ι and $\mathcal{A}$.

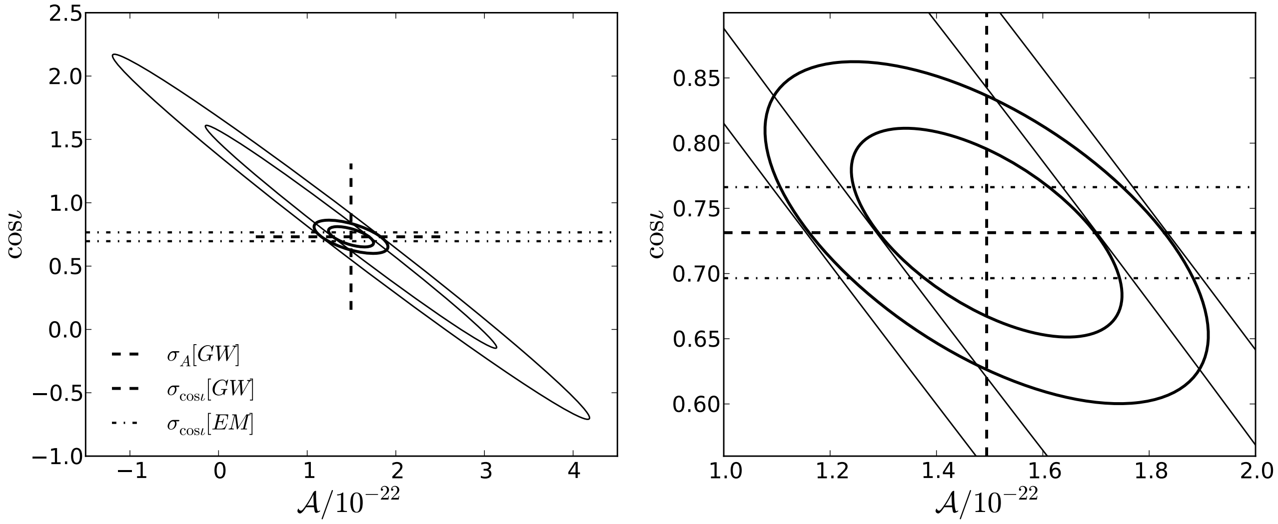

Fig. 2. *Left*: two-dimensional error ellipses of $\mathcal{A}$ and $\cos\iota$ extracted from the variance-covariance matrix, C, for AM CVn. The two thin black lines represent 1-σ and 2-σ ellipses and the black dashed lines represent the 1-σ GW errors in $\mathcal{A}$ and $\cos\iota$ with the cross at the true value of the parameters. The unphysical values (i.e. negative numbers along the amplitude axis) are caused by the Gaussian tails of the parameter uncertainty about their true values. The *right panel* is a zoom of the area that is constrained by the 1-σ EM error of 4° shown in dash-dotted lines. The 1-σ GW standard deviation in $\mathcal{A}$ decreases from $\sim 1.08 \times 10^{-22}$ to $\sim 0.165 \times 10^{-22}$, roughly a factor of 6.5. The corresponding error ellipses for the reduced PDF are shown as thick black ellipses for 1-σ and 2-σ.

strain amplitude $\mathcal{A}$. For example for AM CVn, an EM constraint in ι with a 1-σ accuracy of 4° (Roelofs et al. 2006) improves the uncertainty in $\mathcal{A}$ from 1.084×10^{-22} to 1.65×10^{-23} as shown in Fig. 2. The corresponding 1-σ accuracy in $\mathcal{A}$ is estimated by selecting the two-dimensional probability distribution function (2D PDF) points that lie in the range $41° < \iota < 45°$. This improves amplitude accuracy by a factor of 6.5 compared to the use of GW data alone.

HM Cnc's inclination measurement derived from the EM observation is quite uncertain compared to that for AM CVn. This is mainly due to the large uncertainty in the mass ratio and the assumption about the GW radiation that goes into estimating the inclination (Roelofs et al. 2010). Hence, if we take an EM constraint in ι with a 1-σ uncertainty of 7°, the amplitude improves by a factor of 1.34 as shown in Fig. 3. However, if we were to obtain a better ι constraint of 4° for HM Cnc, $\mathcal{A}$ would improve by a factor of three, which is still a smaller improvement than that of the AM CVn's. This is due to the higher S/N of HM Cnc: if we place AM CVn at a closer distance such that it has a higher S/N of $\sim$40, the 1-σ accuracy of 4° constrains the amplitude more tightly by a factor of 2.95, which is very similar to the case of HM Cnc. By constraining the strain amplitude, we constrain the chirp mass, the distance, or a combination of the two $\frac{\mathcal{M}^{5/3}}{d}$ (see Eq. (3)). The GW frequency, the

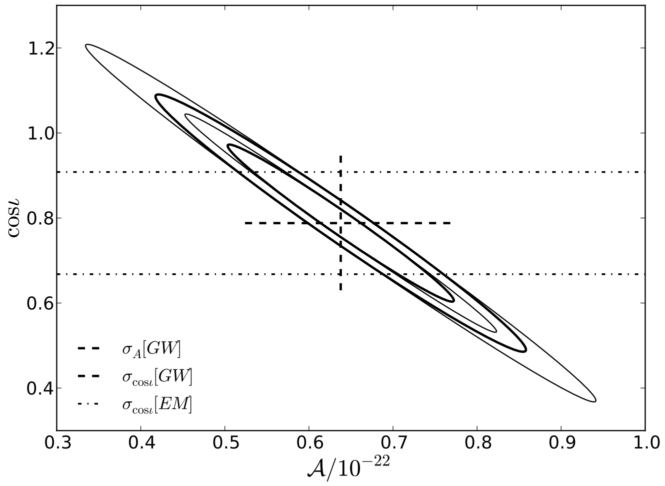

Fig. 3. Two-dimensional error ellipses $\mathcal{A}$ and $\cos\iota$ extracted from the variance-covariance matrix, C, for HM Cnc. See Fig. 2 for details. The 1-σ EM constraint of 7° in inclination reduces the corresponding 1-σ uncertainty in $\mathcal{A}$ from $\sim 1.22 \times 10^{-23}$ to $\sim 0.89 \times 10^{-23}$, roughly a factor of 1.4.

third contributor to the amplitude, is already determined very precisely. Additionally, if $\dot{f}$ is measurable for a chirping binary, then from Eqs. (3) and (4) one can constrain the error in the distance (Schutz 1996).

3.2. Influence of the inclination, ι

We have seen above that $c_{\mathcal{A}\cos\iota}$ depends on the inclination of the binary. For the special case of exactly face-on binaries ($\iota = 0, \pi$), the Fisher matrix is ill-defined owing to the symmetry in the signal, namely, $h(t, \iota + \mathrm{d}\iota) = h(t, \iota - \mathrm{d}\iota)$. The derivatives are zero, so the terms including ι in the Fisher matrix are also zero, resulting in an ill-defined matrix that cannot be inverted. In general, it is hard to track the behaviour of the variance-covariance matrix from the FIM alone. Hence, to determine the influence of inclination, we fix all parameters except $\mathcal{A}$, ι, and λ, and calculate the matrices Γ and C for AM CVn as a function of ι. This can be justified, as most correlations with $\mathcal{A}$ and ι are not very strong; the largest correlation (of ~0.6) is for λ as shown in Fig. 4. This means that for all inclinations

$$C \sim \begin{pmatrix} C_{\mathcal{A}\cos\iota\,\lambda} & 0 \\ 0 & C_{\phi_0\, f\, \psi\, \sin\beta} \end{pmatrix}$$

thus we can focus on $\mathcal{A}$, $\cos\iota$, and λ independently and reduce the 7×7 matrix to a 3×3 matrix, which is easier to interpret[6]. In Fig. 5, we show the S/N, (relative) parameter uncertainties and the normalised correlation for these three parameters as a function of inclination. It is obvious that for a source at a given distance, the S/N for an edge-on binary is lower than that for a face-on binary owing to the less favourable orientation of the latter. Thus, the S/N is a function of $\cos\iota$ and has a minimum at $\iota = 90°$ ($\cos\iota = 0$). In general, we expect the parameter uncertainties to vary accordingly, i.e., a higher S/N should correspond to a higher precision and vice-versa. The longitude follows this behaviour in the bottom-left panel. However, for $\mathcal{A}$ and $\cos\iota$ this is not the case as the detector cannot accurately determine the inclination in the range of $0.7 \lesssim |\cos\iota| \leq 1$, as shown in the top-right and middle-left panels. For $\iota \leq 10°$ and $\iota \geq 170°$ in particular, the uncertainties in ι and $\mathcal{A}$ become very large. However, as shown in the middle-right panel, the correlations are maximal for these almost face-on binaries, thus by constraining one of the parameters from EM (or other) data, we constrain the range of values that the other parameter can take. This method cannot be applied to edge-on binaries as the correlation is very weak in these cases. If we take a value of $\mathrm{d}\iota$ for which the computation of the 3×3 variance-covariance matrix is numerically stable for all ι and use it to produce the full 7×7 matrix, the parameter uncertainties behave as shown in Fig. 6. The uncertainties σ_{ϕ_0} and σ_ψ behave similarly to $\sigma_{\mathcal{A}}$ and σ_ι since ϕ_0, and ψ are also degenerate for nearly face-on systems. In contrast, the uncertainties σ_f, σ_λ, and $\sigma_{\sin\beta}$ behave as may be expected from the S/N since they are not strongly tied to any of the four parameters with strong correlations.

3.3. The correlation between ϕ_0 and ψ

The orientation parameters ϕ_0 and ψ are also highly anti-correlated with $c_{\phi_0\psi} \approx -0.99$ for AM CVn and HM Cnc. This can also be explained by examining the geometry of the physical binary. The orbital phase ϕ is measured in the plane of the binary (perpendicular to the binary's angular momentum vector, $\hat{L}$), while ψ is measured in the plane perpendicular to the line of sight, $\hat{n}$. Both AM CVn and HM Cnc have an inclination in the range where the system appears to be face-on to the detector (see Sect. 3.1). Thus, ϕ_0 and ψ are practically degenerate for these binaries. In contrast, for J0651 $\hat{L}$ and $\hat{n}$ are almost perpendicular, and the effects of ϕ_0 and ψ can be more easily distinguished by eLISA. This correlation is not very noteworthy, because the parameters involved are of little astrophysical interest.

3.4. The correlation between f and ϕ_0

For J0651, there is a strong anti-correlation between f and ϕ_0, with a value of -0.89. This is because if the frequency of a signal is changed by a small fraction, δf, the signal accumulates a phase shift towards the end of the wave. This signal can be deshifted in phase to obtain another signal with a similar match to the original, in turn making the two slightly dissimilar signals indistinguishable. Hence, the two parameters f and ϕ_0 are degenerate. This degeneracy is not present for AM CVn and HM Cnc owing to the strong anti-correlation between ϕ_0 and ψ and large errors in these two parameters.

3.5. The correlation between f and $\dot{f}$

If we model HM Cnc with an additional eighth parameter, $\dot{f}$, we find a strong anti-correlation between f and $\dot{f}$. This can be explained in a very similar way to the case of $c_{f\phi_0}$ above. Consider a signal which is obtained by changing the chirp by $\delta\dot{f}$, within its uncertainty. This will slightly change the frequency towards the end of the signal. By additionally changing f within its uncertainty, we can obtain a very similar signal to the one for which

---

[6] Another reason to consider a smaller matrix is that it is difficult to stabilise C for low inclinations $\iota \leq 10°$. We find that the optimal choice of $\mathrm{d}\theta_i$ for which the parameter uncertainties σ_i are stable varies as a function of inclination. For low values of ι, the optimal $\mathrm{d}\theta_i$ is orders of magnitude larger than for high values of ι. Note that the FIM (as opposed to C) is stable for the same choice of $\mathrm{d}\theta_i$. In addition, the FIM choice of $\mathrm{d}\theta_i$ that is made for the inclination affects only matrix elements that contain terms related to ι. However, this influence spreads to all matrix elements of $C(=\Gamma^{-1})$, because of the matrix inversion.

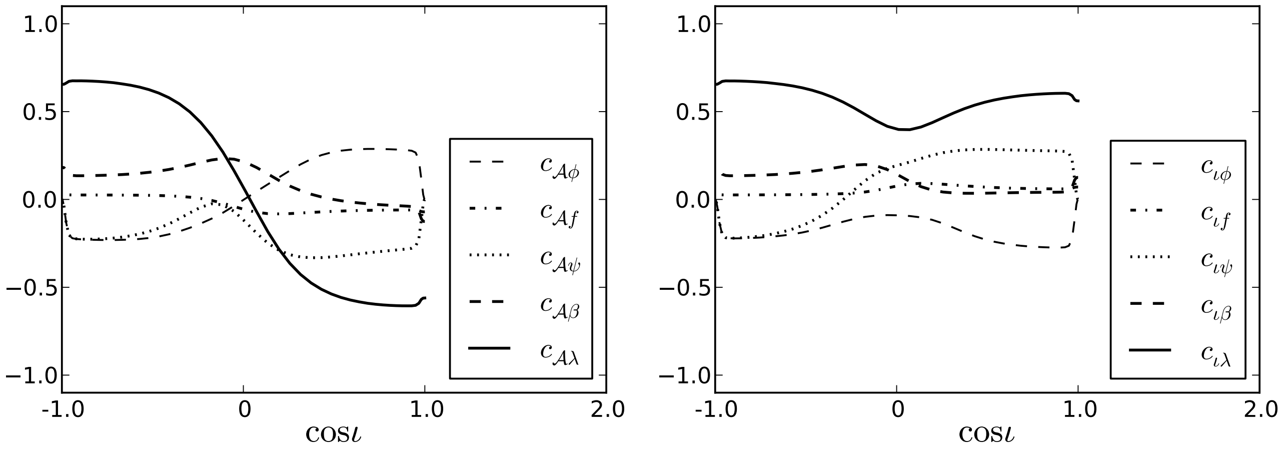

Fig. 4. Correlations of the remaining parameters with $\mathcal{A}$ and ι for a binary with AM CVn's parameter values as a function of $\cos\iota$. Most correlations are weak for all inclinations except $c_{\mathcal{A}\iota}$.

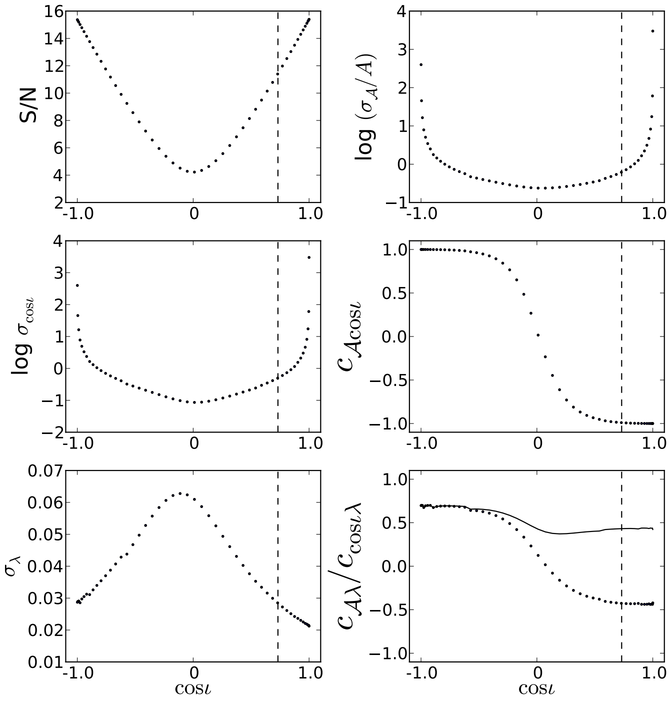

Fig. 5. Signal-to-noise ratio, $\sigma_{\mathcal{A}}$, $\sigma_{\cos\iota}$, σ_λ, $c_{\mathcal{A}\cos\iota}$, $c_{\mathcal{A}\lambda}$, and $c_{\cos\iota\lambda}$ as a function of $\cos\iota$, keeping the other parameters fixed to the values of AM CVn. The vertical dashed line is the measured value of ι for this binary, 43°. The best known value for the amplitude is $\mathcal{A} = 1.49 \times 10^{-22}$. As expected, the S/N is higher for face-on than edge-on orientations. The relative uncertainties in the amplitude and inclination are very large for inclinations up to 10°. The *bottom-right panel* shows the normalised correlations $c_{\mathcal{A}\lambda}$ as the dotted line and $c_{\cos\iota\lambda}$ as the solid line.

we changed only its chirp by $\delta\dot{f}$. Thus, the two parameters are degenerate for a mildly chirping binary. This could be a very useful correlation for constraining the $\dot{f}$ of the binary by using an EM constraint on f. However, the GW data analysis already provides a relative accuracy of $\sim 10^{-6}$ for the frequency, which is hard to improve with EM observations.

After providing a potential measurement of $\dot{f}$ for the J0651 source (M. Kilic, priv. comm.), the correlation between f and $\dot{f}$ could be used to test one of the predictions of General Relativity in Eq. (4), which holds for a binary that evolves only because of GW radiation loss. Given that the individual masses and their f are measured, Eq. (4) can be used to test the prediction of $\dot{f}$.

4. Discussion

The S/N of the data for the verification binaries listed in Table 1 are relatively low. In particular, J0651 has $S/N \sim 10$. This may not satisfy $S/N \gg 1$, one of the criteria under which FIM studies are valid. To exclude the effects of S/N, we place the verification binaries at a closer distance so that they all have S/N of ~100. We find that all of the parameter uncertainties decrease as expected, except for the uncertainty in $\mathcal{A}$. However, the strong correlations we found for $c_{\mathcal{A}\iota}$, $c_{\phi_0\psi}$, $c_{f\phi_0}$ and $c_{f\dot{f}}$ listed above in the matrices remain the same. Furthermore, these correlations do not change when we consider the *six-link* configuration of the classic LISA with a five million km baseline and slightly different instrumental noise. From the *six-link* interferometer, three independent data streams can be synthesised, of which *A, E,* and *T* is one of the combinations. Naturally, this means that the S/N of the source will be higher, and that there may be additional information from these data streams. However, we found that when we consider these optimal TDIs, the strong correlations we found are unaffected. Additionally, the weak correlations between the rest of the parameters are also unaffected.

It is well-known that in the low-frequency regime there are many overlapping sources, which can significantly degrade the parameter uncertainty. Crowder & Cornish (2004) performed a thorough FIM analysis and show that the degradation of parameter uncertainties depends on the frequency, the number of binaries per frequency bin, and the observation time. However, the degradation is uniform for all the seven parameters, which means that each parameter is affected in the same way by the overlapping sources. Hence, the presence of overlapping sources affects the *uncertainties* in the parameters, but not the normalised *correlation* between the parameters. In addition the potential biases from imperfect subtraction of resolvable sources (Sect. 2.3) can affect the results, although this mostly affects the S/N degradation of the source and thus not the normalised correlations.

Our study should be used to implement EM priors in an MCMC data analysis based on a Bayesian framework. While the latter leads to more accurate results, the FIM tools provides useful predictions (Vallisneri 2008). In the case of Galactic binaries, it has been shown that the one-dimensional marginalised posterior PDFs are well-matched by the FIM predictions when

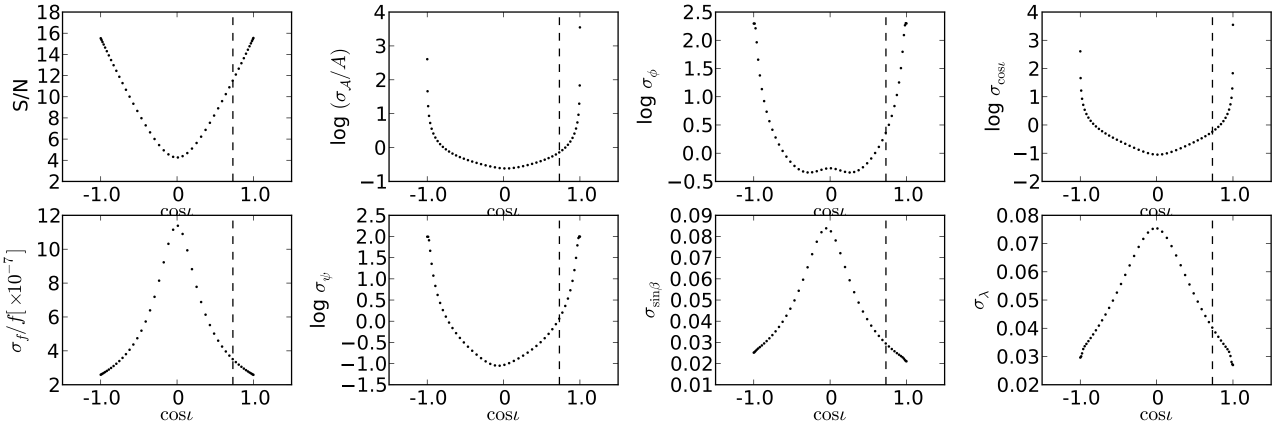

Fig. 6. Signal-to-noise ratio and (relative) parameter uncertainties for AM CVn as a function of $\cos\iota$. The general behaviour for $\sigma_{\mathcal{A}}$, $\sigma_{\cos\iota}$ and σ_{λ} is consistent with Fig. 5 above. The uncertainties in $\sigma_{\sin\beta}$, σ_{λ}, and σ_f behave as may be expected from the S/N, where parameters are more accurately determined for higher S/N.

the data analysis of a single source is considered (Cornish & Crowder 2005).

In a forthcoming paper, we will discuss the dependence of the aforementioned correlations and accuracies on the sky position and polarisation angle. Our test calculations show that the strong correlations $c_{\mathcal{A}\iota}$, $c_{\phi_0\psi}$, $c_{f\phi_0}$, and $c_{f\dot{f}}$ found above do not vary as a function of these parameters.

Finally, we observe that the uncertainty in the inclination of a binary indicates whether the system is eclipsing. In Sect. 3.1, we found that for J0651, the uncertainties in ι, ϕ_0, and ψ are small compared to those of HM Cnc, even though its S/N is a factor of three lower than that of HM Cnc. An uncertainty of $\sigma_{\cos\iota} = 0.043$ translates to $\sigma_\iota \sim 2.5°$. Hence, for J0651-like systems with S/N of $\gtrsim$10, the small uncertainty inclination inferred from a GW analysis may be used to find candidate eclipsers.

5. Conclusion

We have performed Fisher-matrix studies to investigate whether there are correlations between the parameters that characterise Galactic binaries with short periods, between about six minutes and a few hours, which lie in the eLISA frequency band, 10^{-4} Hz−1 Hz. We focused on three verification binaries, AM CVn, SDSS J0651+2844, and the mildly chirping HM Cnc. Our main findings are:

1. There are strong correlations between the strain amplitude and inclination, and between the phase and polarisation angle for AM CVn and HM Cnc. For the latter, there is an additional strong anti-correlation between f and $\dot{f}$ when it is modelled as a mildly chirping source.
2. The remaining parameters are not or only weakly correlated for the binaries considered.
3. The correlation between strain amplitude and inclination can be very useful in constraining the amplitude of the binary, which is a function of the two masses, the distance to the binary, and its frequency. Since the frequency is very accurately determined (of the order of 10^{-9} Hz) by the GW data analysis, a combination of the masses and the distance can be constrained by using an EM constraint on the inclination.
4. These correlations depend strongly on the inclination of the system: approximately face-on ($\iota \lesssim 45°$, $\iota \gtrsim 135°$) binaries have strongly correlated parameters, whereas for edge-on binaries, the correlations become very weak.
5. For binaries with very low inclinations ($\iota < 10°$ and $\iota > 170°$), the uncertainties in amplitude, inclination, phase, and polarisation angle derived from GW data are very large.
6. We have found that the influence of S/N on the correlations is not significant; placing the sources at shorter distances to give them higher S/N yields the same normalised correlations.
7. The strong correlation between amplitude and inclination is the most useful correlation found, since inclinations are typically measured to a higher accuracy by EM observations than with GW measurements alone. Hence, this correlation can be used to constrain the amplitude by a factor of six for systems with orientations and S/N similar to those of AM CVn.
8. We have found that some correlations also depend on sky position and polarisation angle, which we will discuss in a forthcoming paper.
9. Even for signals with an S/N of ∼10, we have been able to reliably determine the inclination when the system is edge-on. This will enable efficient searches for eclipsing systems with EM instruments.

Acknowledgements. This work was supported by funding from FOM. We are very grateful to Michele Vallisneri for providing support with the *Synthetic LISA* and *Lisasolve* softwares. We thank the anonymous referee for the helpful suggestions to improve the paper.

Appendix A: Stabilisation of the variance-covariance matrix

Here we give an example of the Stabilisation of the variance-covariance matrix for AM CVn. The $d\theta_i$ are varied for each parameter over seven orders of magnitude as described in Sect. 2.4. In this example, $d\theta_{\mathcal{A}}$, $d\theta_f$, $d\theta_\iota$, $d\theta_\psi$ are varied from $(10^{-4}, ..., 10^2) \times \sqrt{\epsilon} \times \theta_i$, where, θ_i are the true values for AM CVn. The values of $d\theta_\phi$, $d\theta_\beta$, $d\theta_\lambda$ are varied from $10^{-6}, ..., 10^0$, more than for parameters above, because the numerical derivatives of ϕ, β, and λ are unstable for lower values. The first row of the uncertainties in the parameters correspond to the first set of $d\theta_i$, et cetera. In principle, the uncertainties σ_i should level off around the third row. The uncertainties for all our verification binaries are calculated in this way.

Table A.1. Parameter uncertainties, σ_i, in a range of $d\theta_i$ for the case of AM CVn, with $S/N \sim 11$ for $T_{\rm obs} = 2$ years.

$\sigma_{\mathcal{A}}$	σ_ϕ	$\sigma_{\cos\iota}$	σ_f	σ_ψ	$\sigma_{\sin\beta}$	σ_λ
1.417×10^{-23}	0.317	0.072	6.517×10^{-10}	0.128	0.027	0.029
7.934×10^{-23}	1.693	0.426	6.533×10^{-10}	0.846	0.028	0.034
1.037×10^{-22}	2.234	0.555	6.541×10^{-10}	1.120	0.028	0.038
1.041×10^{-22}	2.242	0.557	6.541×10^{-10}	1.124	0.028	0.039
1.041×10^{-22}	2.242	0.557	6.541×10^{-10}	1.124	0.028	0.039
1.035×10^{-22}	2.250	0.554	6.556×10^{-10}	1.126	0.029	0.04
8.756×10^{-23}	2.301	0.473	8.259×10^{-10}	0.942	0.113	0.122

Notes. The values start to level off from the third to fifth row.

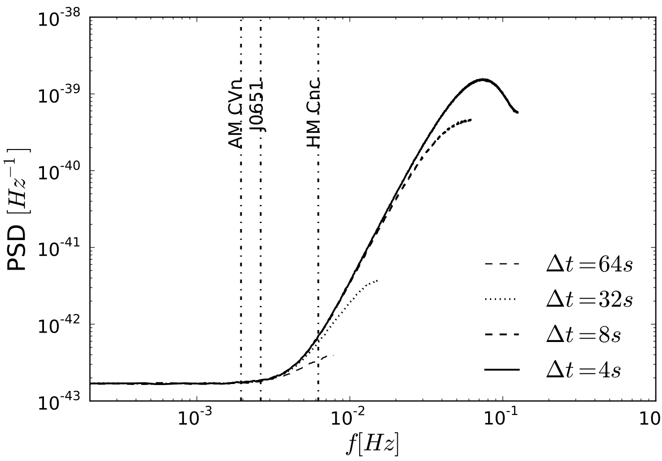

Fig. B.1. Average PSDs of instrumental noise for eLISA with varying sampling time, Δt. For lower-frequency sources such as AM CVn and J0651, a sampling as fine as 64 s can be used. However, for HM Cnc, whose frequency is higher, a high Δt would overestimate its S/N, since the level of the noise is too low for the longest sampling times.

Appendix B: Sampling

In Fig. B.1, we show the effect of the sampling time Δt on the noise PSD of the instrumental noise, which is the average spectrum of the TDI X observable. At $f < 5 \times 10^{-3}$ Hz, the sampling time does not affect the level of the PSD. Above these frequencies, the PSD with a relatively long sampling time of 64 s underestimates its true level.

References

Amaro-Seoane, P., Aoudia, S., Babak, S., et al. 2012, GW Notes, submitted [arXiv:1201.3621]
Armstrong, J. W., Estabrook, F. B., & Tinto, M. 1999, ApJ, 527, 814
Brown, W. R., Kilic, M., Hermes, J. J., et al. 2011, ApJ, 737, L23
Cornish, N. J., & Crowder, J. 2005, Phys. Rev. D, 72, 043005
Cornish, N. J., & Larson, S. L. 2003, Class. Quant. Grav., 20, 163
Cornish, N. J., & Littenberg, T. B. 2007, Phys. Rev. D, 76, 083006
Cornish, N. J., & Rubbo, L. J. 2003, Phys. Rev. D, 67, 022001
Cutler, C. 1998, Phys. Rev. D, 57, 7089
Cutler, C., & Flanagan, É. E. 1994, Phys. Rev. D, 49, 2658
Finn, L. S. 1992, Phys. Rev. D, 46, 5236
in't Zand, J. J. M. 2005, A&A, 441, L1
Królak, A., Tinto, M., & Vallisneri, M. 2004, Phys. Rev. D, 70, 022003
LISA Study Team. 1998, LISA: Laser Interferometer Space Antenna for the Detection and Observation of Gravitational Waves, Pre-Phase A Report, 2nd edn. (Garching, Germany: Max Planck Institut fur Quantenoptik)
Littenberg, T. B. 2011, Phys. Rev. D, 84, 063009
Nelemans, G. 2009, Class. Quant. Grav., 26, 094030
Nelemans, G. 2011, Wiki Verification Sources
Nelemans, G., Yungelson, L. R., & Portegies Zwart, S. F. 2001, A&A, 375, 890
Nelemans, G., Yungelson, L. R., & Portegies Zwart, S. F. 2004, MNRAS, 349, 181
Nissanke, S., Vallisneri, M., Nelemans, G., & Prince, T. A. 2012, ApJ, submitted [arXiv:1201.4613]
Petiteau, A. 2012, Configurations of the eLISA (NGO) mission
Press, W. H., Teukolsky, S. A., Vetterling, W. T., & Flannery, B. P. 2002, Numerical recipes in C++: the art of scientific computing, eds. W. H. Press, S. A. Teukolsky, W. T. Vetterling, & B. P. Flannery
Roelofs, G. H. A., Groot, P. J., Nelemans, G., Marsh, T. R., & Steeghs, D. 2006, MNRAS, 371, 1231
Roelofs, G. H. A., Groot, P. J., Benedict, G. F., et al. 2007, ApJ, 666, 1174
Roelofs, G. H. A., Rau, A., Marsh, T. R., et al. 2010, ApJ, 711, L138
Schutz, B. F. 1996, Class. Quant. Grav., 13, A219
Skillman, D. R., Patterson, J., Kemp, J., et al. 1999, PASP, 111, 1281
Solheim, J.-E. 2010, PASP, 122, 1133
Stroeer, A., & Vecchio, A. 2006, Class. Quant. Grav., 23, 809
Strohmayer, T. E. 2005, ApJ, 627, 920
Takahashi, R., & Seto, N. 2002, ApJ, 575, 1030
Timpano, S. E., Rubbo, L. J., & Cornish, N. J. 2006, Phys. Rev. D, 73, 122001
Vallisneri, M. 2005a, Phys. Rev. D, 72, 042003
Vallisneri, M. 2005b, Phys. Rev. D, 71, 022001
Vallisneri, M. 2008, Phys. Rev. D, 77, 042001
Vallisneri, M. 2011, Lisasolve fastbinary package
Vallisneri, M., Crowder, J., & Tinto, M. 2008, Class. Quant. Grav., 25, 065005
Webbink, R. F. 1984, ApJ, 277, 355